Human Molecular Genetics, 2020, Vol. 29, No. 3 418–431

doi: 10.1093/hmg/ddz298
Advance Access Publication Date: 24 December 2019
General Article One

GENERAL ARTICLE ONE

Mutant huntingtin interacts with the sterol regulatory element-binding proteins and impairs their nuclear import

Alba Di Pardo[1,†], John Monyror[1,§], Luis Carlos Morales[1,‡,§], Vaibhavi Kadam[1,2], Susanne Lingrell[1], Vittorio Maglione[1,†], Richard W. Wozniak[3] and Simonetta Sipione[1,2,*]

[1]Department of Pharmacology, University of Alberta, Edmonton, AB, T6G 2H7, Canada, [2]Neuroscience and Mental Health Institute, University of Alberta, Edmonton, AB, T6G 2H7, Canada, and [3]Department of Cell Biology, University of Alberta, Edmonton, AB, T6G 2H7, Canada

*To whom correspondence should be addressed. Tel: +1-780-492-5885; Fax: +1-780-492-4325; Email: ssipione@ualberta.ca

Abstract

Brain cholesterol homeostasis is altered in Huntington's disease (HD), a neurodegenerative disorder caused by the expansion of a CAG nucleotide repeat in the *HTT* gene. Genes involved in the synthesis of cholesterol and fatty acids were shown to be downregulated shortly after the expression of mutant huntingtin (mHTT) in inducible HD cells. Nuclear levels of the transcription factors that regulate lipid biogenesis, the sterol regulatory element-binding proteins (SREBP1 and SREBP2), were found to be decreased in HD models compared to wild-type, but the underlying causes were not known. SREBPs are synthesized as inactive endoplasmic reticulum-localized precursors. Their mature forms (mSREBPs) are generated upon transport of the SREBP precursors to the Golgi and proteolytic cleavage, and are rapidly imported into the nucleus by binding to importin β. We show that, although SREBP2 processing into mSREBP2 is not affected in YAC128 HD mice, mSREBP2 is mislocalized to the cytoplasm. Chimeric mSREBP2-and mSREBP1-EGFP proteins are also mislocalized to the cytoplasm in immortalized striatal cells expressing mHTT, in YAC128 neurons and in fibroblasts from HD patients. We further show that mHTT binds to the SREBP2/importin β complex required for nuclear import and sequesters it in the cytoplasm. As a result, HD cells fail to upregulate cholesterogenic genes under sterol-depleted conditions. These findings provide mechanistic insight into the downregulation of genes involved in the synthesis of cholesterol and fatty acids in HD models, and have potential implications for other pathways modulated by SREBPs, including autophagy and excitotoxicity.

Introduction

Huntington's disease (HD) is an inherited neurodegenerative protein misfolding disease characterized by progressive motor, cognitive and psychiatric symptoms. The underlying cause is a mutation in the *HTT* gene, which results in the pathological expansion of a polyglutamine (polyQ) stretch at the N-terminus of the huntingtin (HTT) protein (1,2). Misfolding and aggregation of mutant HTT (mHTT) triggers a wide array of cellular and metabolic dysfunctions culminating in

[†]Current address: IRCCS Neuromed, Pozzilli (IS), Italy
[‡]Current address: Department of Medicine, Universidad del Norte, Barranquilla, Colombia
[§]Equal contribution

Received: August 12, 2019. **Revised:** November 14, 2019. **Accepted:** December 5, 2019

neurodegeneration, mainly in the brain cortex and in the corpus striatum (3–5).

Transcriptional downregulation of enzymes required for the synthesis of cholesterol (mevalonate pathway) and fatty acids is one of the early dysfunctions occurring in HD, identified first in an inducible cell model expressing mHTT under control of a doxycycline-inducible promotor (6). Downregulation of the mevalonate pathway was later confirmed in a wide range of HD animal models and in fibroblasts and post-mortem brains from HD patients (7–10).

The mevalonate pathway is responsible for the synthesis of cholesterol and isoprenoids, lipids with crucial roles in a variety of cellular processes. Isoprenoids are used for protein prenylation and as precursors for the synthesis of coenzyme Q and dolichol. They are therefore important for cell signaling, vesicle trafficking, mitochondrial energy metabolism and protein glycosylation (11–13). Cholesterol is a major component of myelin (14), the precursor for the synthesis of neurosteroids (15,16), and a crucial modulator of membrane properties (17–20), synaptogenesis and synaptic transmission (21–25). Cholesterol is also the substrate for the synthesis of 24(S)-hydroxy-cholesterol, a known ligand for the liver X receptor (LXR), activation of which results in regulation of brain cholesterol homeostasis as well as anti-inflammatory and neuroprotective effects (26).

Because dietary and peripherally synthesized cholesterol cannot cross the blood–brain barrier (14), local *de novo* cholesterol synthesis is crucial to maintain the brain cholesterol pool, which accounts for up to 25% of all cholesterol in the body (27). It is therefore not surprising that mutations that affect the mevalonate pathway or cholesterol cellular distribution cause severe neurodevelopmental and neurodegenerative disorders (28,29). In HD, downregulation of the mevalonate pathway results in decreased *de novo* synthesis of cholesterol in cells and brains of animal models (7,8,10,30), decreased supply of cholesterol-containing lipoproteins from HD astrocytes to neurons (31) and decreased synaptogenesis and neurite outgrowth (31). In line with these findings, administration of exogenous cholesterol was shown to increase synaptogenesis in HD neurons *in vitro* (31) and to improve synaptic activity and cognitive functions *in vivo* in HD mice (32). Altogether, these data support the hypothesis that changes in gene expression that decrease the activity of the mevalonate pathway contribute to HD pathogenesis and/or progression.

Expression of cholesterogenic and other lipid-related genes is regulated by the sterol regulatory element-binding proteins (SREBPs), basic helix-loop-helix leucine zipper (bHLH-LZ) transcription factors that bind to sterol regulatory elements (SRE) in the Promoter of target genes. Of the three mammalian SREBP isoforms, SREBP1a, (mainly expressed in rapidly proliferating cells) has the broadest activity, regulating the synthesis of both cholesterol and fatty acids; SREBP1c controls fatty acid and triacylglycerol synthesis, while SREBP2 regulates cholesterol synthesis and metabolism in all tissues (33,34). All three isoforms are expressed as transcriptionally inactive transmembrane precursors that are retained in the endoplasmic reticulum (ER) membrane through their interaction with the SREBP cleavage-activating protein (SCAP). SCAP works as a cholesterol sensor and, as long as the ER sterol levels are high, it remains anchored in the ER membrane through its interaction with the insulin-induced gene (Insig) proteins. In low ER sterol conditions, SCAP dissociates from Insigs and escorts SREBPs to the Golgi. Here, site-1 protease (S1P) and site-2 protease (S2P) sequentially cleave SREBPs releasing their transcriptionally active bHLH-LZ-containing N-terminal domain (mature SREBP, mSREBP) (35,36), which is then delivered to the nucleus via direct interaction with importin β (37–39).

Transcriptional targets of both SREBP2 and SREBP1 were found to be downregulated in inducible cells expressing mHTT (6) and decreased amounts of mSREBPs were reported in the nucleus of HD models (9,31), but until now, the underlying causes have remained elusive. In this study, we show that mHTT binds to mSREBPs in a complex with importin β and impairs mSREBPs nuclear translocation. As a result, HD cells fail to upregulate cholesterogenic genes when sterol supply is limited or when the activity of the mevalonate pathway is inhibited by statins.

Results

Altered subcellular distribution of mature SREBP2 in the cerebral cortex of YAC128 mice

To investigate the mechanism underlying downregulation of cholesterogenic genes in HD, we analyzed the expression and subcellular distribution of SREBP2 and the abundance of its transcriptionally active cleaved form (mature SREBP2, mSREBP2) in brain tissue obtained from YAC128 mice, a well-characterized transgenic model of HD. These mice express the entire human HD gene with 128 CAG repeats and recapitulate many aspects of the human pathology (40). In the cortex and striatum of symptomatic 6-month-old YAC128 mice, total levels of the SREBP2 precursor protein (pSREBP2, Fig. 1A) and mature SREBP-2 (mSREBP-2, Fig. 1B) were comparable to WT littermates, suggesting that SREBP2 processing is not affected in YAC128 mice. However, following subcellular fractionation of cortical tissue, we observed an abnormal enrichment of mSREBP2 in the cytoplasmic fraction in YAC128 compared to WT mice (Fig. 1B), suggesting that nuclear localization of mSREBP2, rather than its production through cleavage of the precursor protein, might be affected in the cerebral cortex of HD mice. No differences in the intracellular distribution of mSREBP2 were observed in the striatum of 6-month-old YAC128 mice compared to controls (Fig. 1B).

Aberrant intracellular localization of mSREBP2- and mSREBP1c-EGFP in cells expressing mHTT

To further investigate the intracellular localization of mSREBP2 in HD, we expressed a chimeric mSREBP2-EGFP protein in immortalized rat striatal cells (ST14A) constitutively expressing the N-terminal region of either wild-type (N548-15Q) or mHTT (N548-128Q). Inducible expression of this pathogenic mHTT fragment was previously shown to result in the downregulation of SREBP target genes in the same cells (41). Expression of mSREBP2-EGFP in transfected cells was higher in parental ST14A cells, but comparable between N548-15Q and N548-128Q cells (Fig. 2A). In parental cells and in cells overexpressing wild-type HTT, mSREBP2-EGFP was localized in the nucleus, as expected (Fig. 2B). In cells overexpressing mHTT, mSREBP2-EGFP was detected both in the nucleus and in the cytoplasm (Fig. 2B and relative quantification in Fig. 2C). Aberrant localization of the chimeric protein was also observed in knock-in cells expressing endogenous levels of full-length mHTT ($STHdh^{111/111}$) (Fig. 2C), in primary cortical YAC128 neurons (Fig. 2D) and in fibroblasts isolated from HD patients, compared to control cells (Figs 2E and 4D). Subcellular fractionation of knock-in $STHdh^{111/111}$ cells confirmed mislocalization of mSREBP2 in the cytoplasmic fraction (Fig. 2F). Altogether, these data suggest that mislocalization of mSREBP2 occurs in murine as well as

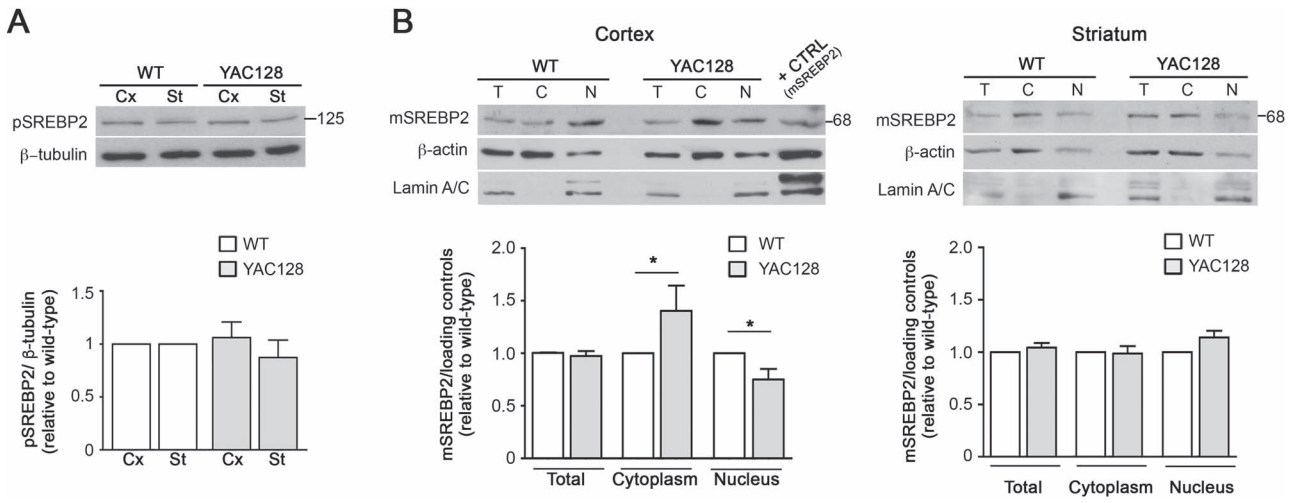

Figure 1. Decreased nuclear enrichment of mature SREBP2 in cortical tissue from YAC128 mice compared to WT. (**A**) Representative immunoblot for the precursor form of SREBP2 (pSREBP2) in total lysates of 6-month-old WT and YAC128 cerebral cortex (Cx) and striatum (St). The graph shows the mean densitometric values ± SD of four mice per genotype. (**B**) Representative immunoblots and relative densitometric analysis for the mature form of SREBP2 (mSREBP2) in total lysates (T) and in cytoplasmic (C) and nuclear (N) fractions prepared from cortical and striatal tissue from WT and YAC128 mice. The last lane on the immunoblot shows a positive control (+ CTRL) generated by transient transfection of STHdh7/7 cells with mSREBP2 cDNA. Graphs show the densitometric analysis of three independent experiments. ß-actin and lamin A/C were used as loading controls for cytoplasmic and nuclear fractions, respectively. Two-tailed *t*-test, $^{*}P < 0.05$.

human models of HD, in cells expressing transgenic or endogenous mHTT and in HD cells of neuronal and non-neuronal origin.

Similar to mSREBP2, mSREBP1c-EGFP was also mislocalized to the cytoplasm in HD models, including human HD fibroblasts (Fig. 3A) and immortalized striatal cells (Fig. 3B), in spite of similar expression of the chimeric protein in transfected cells (Fig. 3C). On the contrary, EGFP containing a classic nuclear localization signal (NLS-EGFP) was correctly targeted to the nucleus (Fig. 3D), suggesting that mHTT specifically interferes with nuclear localization of both SREBPs, but not with classic nuclear import, at least in our models.

Mature SREBP2 interacts with soluble mHTT but is not entrapped in mHTT aggregates

Several proteins and transcription factors are sequestered within mHTT aggregates (42). To determine whether mSREBPs were trapped into insoluble mHTT aggregates in the cytoplasm of HD cells, we performed filter-trap assay on cellular lysates after transfection of N548-128Q cells with mSREBP2-EGFP. SDS-insoluble aggregates of mHTT were trapped on a cellulose acetate filter and detected by immunoblotting; however, no mSREBP2-EGFP2 was detected on the filter (Fig. 4A), suggesting that the transcription factor is not trapped into SDS-insoluble aggregates. In line with these findings, after SDS-PAGE separation of cell lysates, no mSREBP2-EGFP could be detected in the stacking gel, where insoluble mHTT is found (Fig. 4B). Confocal microscopy after cell immunostaining with EM48, an antibody specific for mHTT aggregates, confirmed the absence of significant colocalization between mSREBP2-EGFP and EM48 immunoreactivity (Fig. 4C). Instead, in primary human HD fibroblasts, most mSREBP2-EGFP colocalized with non-aggregated HTT (detected with mAb2166 antibodies, Fig. 4D).

To determine whether mSREBP2 and HTT interact with each other, we transfected and immunoprecipitated mSREBP2-EGFP from the cytoplasmic fraction of various HD cell models. Mutant HTT co-immunoprecipitated with mSREBP2-EGFP from N548-128Q cytoplasmic fractions. The interaction was specific for mSREBP2, as no mHTT was co-immunoprecipitated from cells expressing EGFP only (Fig. 5A). The wild-type N548-15Q fragment also co-immunoprecipitated with mSREBP2-EGFP, but to a much lesser extent than the mutant protein (Fig. 5A). Similar results were obtained using cytoplasmic fractions from knock-in striatal cells that express endogenous levels of full-length HTT (Fig. 5B). When immunoprecipitation was performed from nuclear fractions, both wild-type and mutant HTT co-immunoprecipitated with mSREBP2-EGFP to a similar extent (Fig. 5C), suggesting that HTT might be part of a transcriptional complex with mSREBP2 in the nucleus of healthy cells (see further discussion below). Importantly, endogenous mSREBP2 co-immunoprecipitated with mHTT from the cytoplasmic fraction of cortical YAC128 brain tissue (Fig. 5D) suggesting that the interaction is not an artifact of models of SREBP2 overexpression and occurs *in vivo*. Altogether, our data suggest that soluble mHTT binds mSREBP2 in the cytoplasm of HD cells and this interaction may prevent nuclear import of mSREBP2.

Mutant HTT binds mSREBP2 and stabilizes the interaction between mSREBP2 and importin β

The mature forms of SREBPs do not contain a classic nuclear localization signal (NLS) and translocate to the nucleus via direct binding to one of the HEAT domains of importin β (37). Named from the four proteins where they were first described (Huntingtin, Elongation factor 3, A subunit of PP2A and TOR1), HEAT domains consist of flexible arrays of amphiphilic α-helices and are involved in protein–protein interactions (43). Since HTT contains two large HEAT domains (one of them encompassing the N-terminal region of the protein) (44), we hypothesized that mHTT binding to mSREBPs through its N-terminal HEAT domain might prevent the formation of the mSREBP/importin β complex required for nuclear translocation. To test this hypothesis, we measured the amount of importin β that

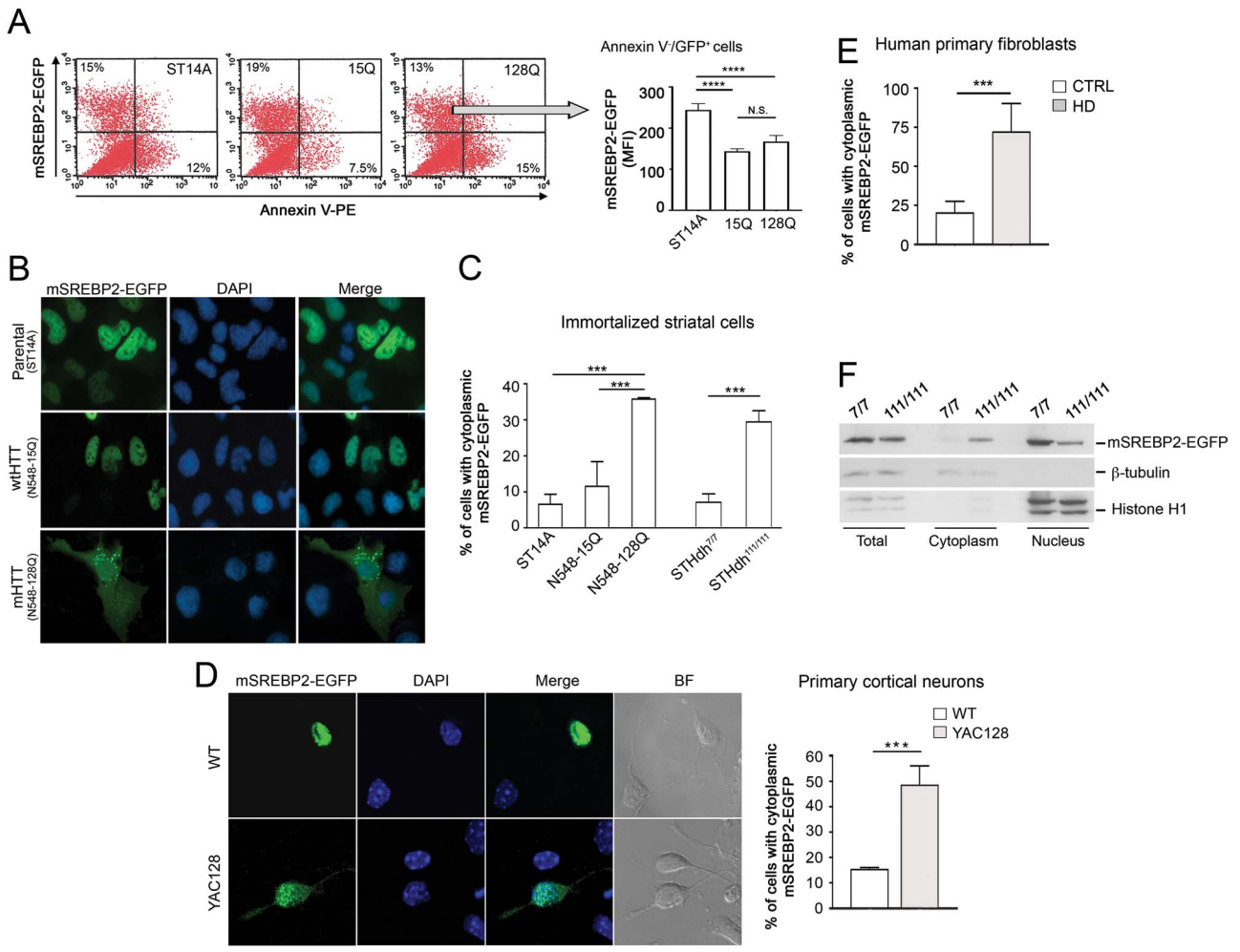

Figure 2. mSREBP2-EGFP is mislocalized to the cytoplasm of HD cells. (**A**) Representative scatter plots and analysis of mSREBP2-EGFP transfection in parental striatal cells (ST14A) and in cells constitutively expressing an N-terminal fragment of wild-type (N548-15Q, abbreviated as 15Q) or mutant HTT (N548-128Q, abbreviated as 128Q). Mean transfection efficiency is shown in the upper left quadrants. Mean mSREBP2-EGFP expression in transfected cells is shown in the graph. Annexin V^+-cells (apoptotic) were excluded from the analysis. $N = 3$. One-way ANOVA with Tukey's multiple comparison test. (**B**) Representative confocal microscopy images showing the intracellular localization of transiently transfected mSREBP2-EGFP in. Cell nuclei were counterstained with DAPI. Quantification is shown in C. (**C**) Quantification of cells with cytoplasmic localization of mSREBP2-pEGFP. A minimum of 80 mSREBP2-EGFP expressing-cells per cell line were counted in each of three independent experiments. One-way ANOVA and two-tailed *t*-test (for STHdh cells). (**D**) Representative confocal microscopy images of WT and YAC128 cortical neurons (10 DIV) 24 h after transfection with mSREBP2-EGFP. The percentage of neurons with cytoplasmic localization of mSREBP2-EGFP is shown in the bar graph. A minimum of 100 cells per genotype were counted over three independent experiments. BF, bright field. Two-tailed *t*-test. (**E**) Quantification of cells with cytoplasmic localization of mSREBP2-EGFP in transiently transfected human fibroblasts from normal subjects or HD patients. Representative confocal microscopy images are shown in Figure 5D. For each genotype, two independent lines of fibroblasts were analyzed (70–80 cells per line) and data were combined. Two-tailed *t*-test. (**F**) Subcellular fractionation and immunoblotting showing cytoplasmic location of mSREBP2-EGFP in transiently transfected $STHdh^{111/111}$ (111/111) knock-in cells compared to wild-type $STHdh^{7/7}$ (7/7) cells. Tubulin and histone H1 were used as loading controls for total/cytoplasmic and nuclear fractions, respectively. The experiment was repeated twice with similar results. Bar graphs show mean values ± SD. MFI = mean fluorescence intensity. N.S. = not significant. $^{***}P < 0.001$; $^{****}P < 0.0001$.

co-immunoprecipitated with mSREBP2-EGFP from cytoplasmic fractions of cells expressing wild-type or mHTT. Contrary to our prediction (of decreased mSREBP binding to importin β), immunoprecipitation with an anti-GFP antibody showed more importin β co-immunoprecipitating with mSREBP2-EGFP from cells expressing mHTT (N548-128Q) than from wild-type (N548-15Q) cells, despite the fact that the overall expression of importin β was similar between the two cell lines (input, Fig. 6A). In our experimental conditions, the low levels of importin β that co-immunoprecipitated with mSREBP2-EGFP from wild-type cytoplasmic fractions are likely explained by the fact that, in normal conditions, the importin β-mSREBP complex is rapidly imported into the nucleus. Here, the binding of nuclear Ran-GTP to importin β would dissociate the complex, thus maintaining steady state levels of the importin β-mSREBP complex at low levels in the cell. The observed increase of importin β bound to mSREBP2 in the cytoplasm of HD cells suggests that mHTT, which co-immunoprecipitated with mSREBP2 and importin β (Fig. 6A), impairs nuclear import of the complex or Ran-GTP-stimulated release of importin β from mSREBP. Similar results were obtained in knock-in cells expressing endogenous levels of full-length mHTT (Fig. 6B), thus excluding the possibility of artifacts due to mHTT overexpression.

To further assess the role of mHTT in the mHTT-mSREBP-importin β complex, we also examined the consequences of incubating the isolated complex (obtained by immunoprecipitation using anti-GFP antibodies) with recombinant RanGTP.

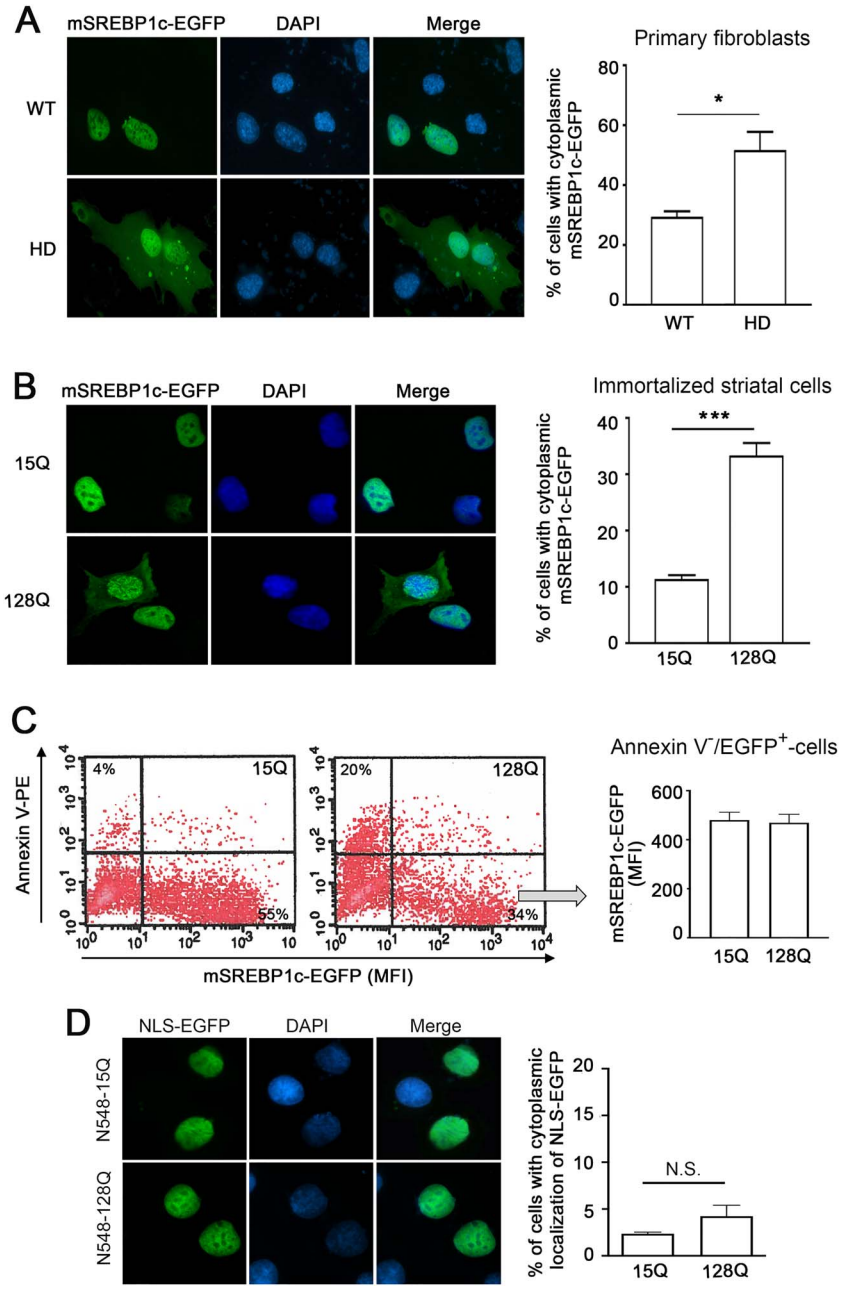

Figure 3. mSREBP1c-EGFP is mislocalized to the cytoplasm in HD cells. **(A)** Representative confocal microscopy images showing the intracellular localization of transfected mSREBP1c-EGFP in normal and HD human primary fibroblasts. The graph shows the percentage of cells with cytoplasmic localization of the chimeric protein. Two different lines of fibroblasts per genotype were used in three independent experiments (>140 transfected cells were counted for each genotype) and data were combined. **(B)** Representative confocal microscopy images and quantification of cells with cytoplasmic localization of mSREBP1c-EGFP in transiently transfected N548-15Q and N548-Q128 cells from three independent experiments. **(C)** Representative scatter plots and analysis of mSREBP1c-EGFP-transfected cells. Transfection efficiency is indicated by the numbers in the lower right quadrants. mSREBP1c-EGFP mean fluorescence intensity (MFI) was comparable in wild-type (15Q) and HD (128Q) cells. **(D)** Representative confocal microscopy images and analysis of N548-15Q and N548–128Q cells transiently transfected with EGFP fused to a classic nuclear localization sequence (NLS-EGFP). The experiment was repeated twice with similar results. High content analysis of NLS-EGFP subcellular localization was performed on a total of 1613 N548-15Q and 2030 N548-128Q cells. The chimeric protein was detected only in the nucleus in the majority of cells, regardless of cell genotype. Data are means ± SD. Two-tailed *t*-test. $^{*}P < 0.05$; $^{***}P < 0.001$; N.S. = not significant.

As shown in Figure 6C, the addition of Ran-GTP induced the release of importin β into the unbound fraction, while mHTT remained bound to mSREBP2. These results suggest that mHTT does not interfere with the ability of importin β to bind RanGTP and release its cargo. Moreover, the interaction of mHTT with mSREBP2-EGFP is not dependent on the co-binding of importin β.

Sequestration of mSREBP2 in the cytoplasm of HD cells results in decreased expression of target genes

Our studies show that in HD cells, a significant fraction of mSREBPs is not imported into the nucleus. This would be expected to result in decreased expression of SREBP target genes, and might explain why cholesterogenic and other lipid-related genes are expressed at lower levels than normal in

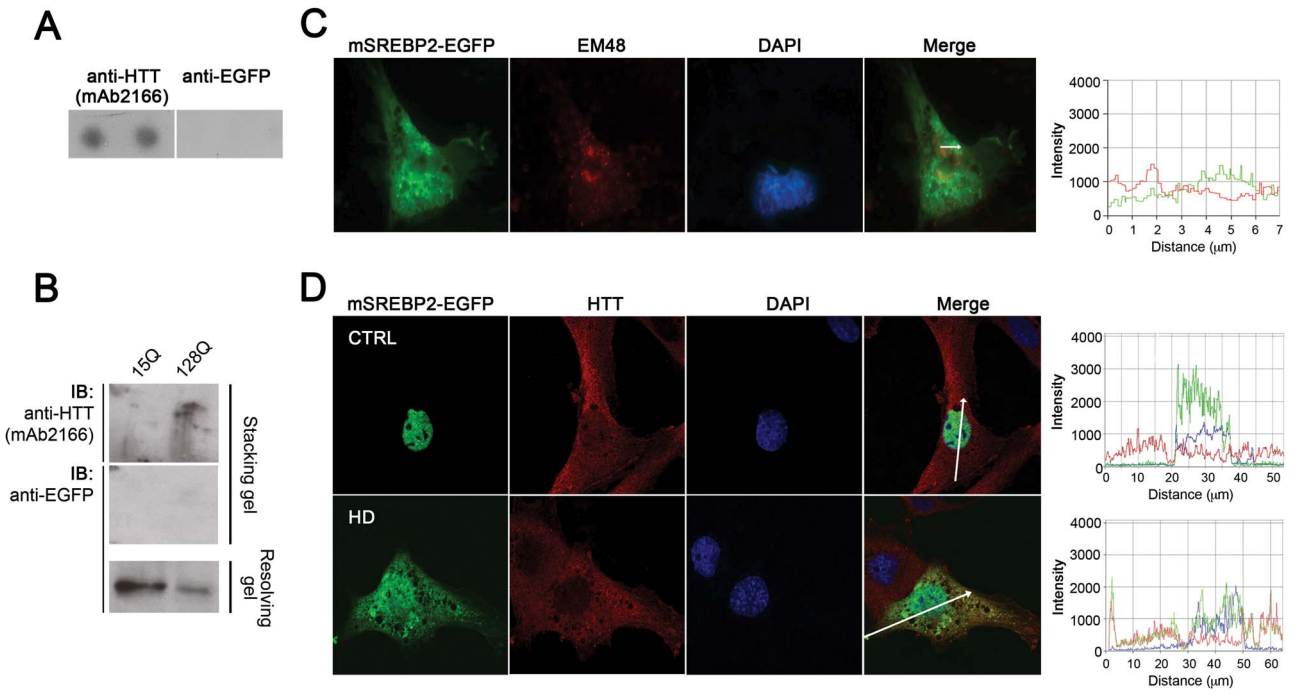

Figure 4. mSREBP2-EGFP co-localizes with mHTT but is not sequestered into insoluble mHTT aggregates. (**A**) Filter trap retention assay performed on total cell lysate from N548-128 cells, 24 h after transfection with mSREBP2-EGFP. Mutant HTT aggregates trapped on a cellulose acetate filter were detected with anti-HTT antibodies (mAb2166). No mSREBP2-EGFP was detected in the insoluble material using anti-GFP antibodies. The experiment was repeated twice with similar results. (**B**) In an independent experiment, total cell lysates of N548-15Q and N548-128Q cells transfected with mSREBP2-EGFP were separated on SDS-PAGE. Insoluble aggregates of mHTT were detected in the stacking gel by immunoblotting. mSREBP2-EGFP was detected only in the resolving gel. (**C**) Representative confocal images and fluorescence intensity profiles of N548-128Q cells transfected with mSREBP2-EGFP and immunostained with EM48 antibodies to detect mHTT aggregates. The line-scan graph shows lack of co-localization between the signal generated by EM48 (red line) and mSREBP2-EGFP (green line). (**D**) Representative confocal microscopy images and fluorescence intensity profiles of primary human fibroblasts transiently transfected with mSREBP2-EGFP and immunostained with anti-HTT antibodies (PW0595). The line-scan graphs show the immunofluorescence intensity of HTT (red line) and mSREBP2-EGFP (green line) signals along the white arrow, and colocalization of mSREBP2-EGFP with HTT in the cytoplasm of HD cells. Experiments were repeated twice with similar results.

HD models (6–10). To test this hypothesis and to investigate the impact of mSREBP mislocalization on gene expression in HD cells, we transfected age-matched human control (C15M) and HD fibroblasts (HD11M) with mSREBP2 and measured the expression of *HMGCR*, an established mSREBP2 target gene that encodes 3-hydroxy-3-methylglutaryl-CoA reductase, the rate limiting enzyme in the mevalonate pathway. The immunoblot in Figure 7A shows the levels of mSREBP2 expression resulting from the transfection of different amounts of cDNA or from the transfection of an 'attenuated' cDNA with reduced translation efficiency due to lack of the canonical Kozak consensus sequence upstream to the start codon (45). The latter allowed for reduced cellular transgene expression without sacrificing overall transfection efficiency. As expected, in all conditions control fibroblasts increased transcription of *HMGCR* over baseline (control EGFP transfection, Fig. 7A). However, HD cells upregulated *HMGCR* to a much lesser extent, especially at lower mSREBP2 levels (Fig. 7A, compare expression at 2.5 μg cDNA and 5 μg Kozak-less cDNA transfection). Results were confirmed by analysis of *HMGCR* mRNA levels in the same fibroblast lines and in two additional others (C33M and HD35M), after fluorescence-activated cell sorting (FACS) of cells co-transfected with mSREBP2 and EGFP (Fig. 7B), which allowed to exclude potential confounding effects from the pool of non-transfected cells. In both HD lines, *HMGCR* mRNA levels were lower than in control fibroblasts, even though mean transgene expression was higher (based on co-transfected EGFP mean fluorescence intensity, MFI = 1.65 ± 0.21 in HD versus 1.025 ± 0.035 in WT, see scatter plots in Fig. 7B). Altogether, our data support the hypothesis that aberrant interaction of mHTT with mSREBP2 leads to decreased transcription of mSREBP2 target genes. Sequestration of mSREBP2 in the cytoplasm would be expected to affect the ability of HD cells to respond to sterol deprivation and other conditions, where SREBPs are normally activated. To test this hypothesis, we cultured human control and HD fibroblasts in lipoprotein-deficient medium (LPDM) for 48 h, which is known to result in cell cholesterol depletion and stimulation of cholesterol synthesis via SREBP-mediated transcription of *HMGCR* (46,47). In these conditions, HD fibroblasts failed to upregulate *HMGCR* mRNA to the same extent as control cells (Fig. 7C). HD cells were also unable to upregulate *HMGCR* expression when grown in the presence of pravastatin, an inhibitor of HMGCR activity and cholesterol synthesis (Fig. 7D).

Discussion

In this study, we have shed light on the mechanism responsible for the downregulation of genes involved in the synthesis of cholesterol and fatty acids in HD (6–10). Expression of these genes was found to be decreased as early as 12–24 h after mHTT expression in an inducible cell model of HD (6). Subsequent studies demonstrated that the resulting downregulation of the mevalonate pathway has significant impact on HD pathogenesis (31,32). Decreased nuclear levels of SREBP1 and SREBP2 were observed in HD models (7), but it remained unclear whether

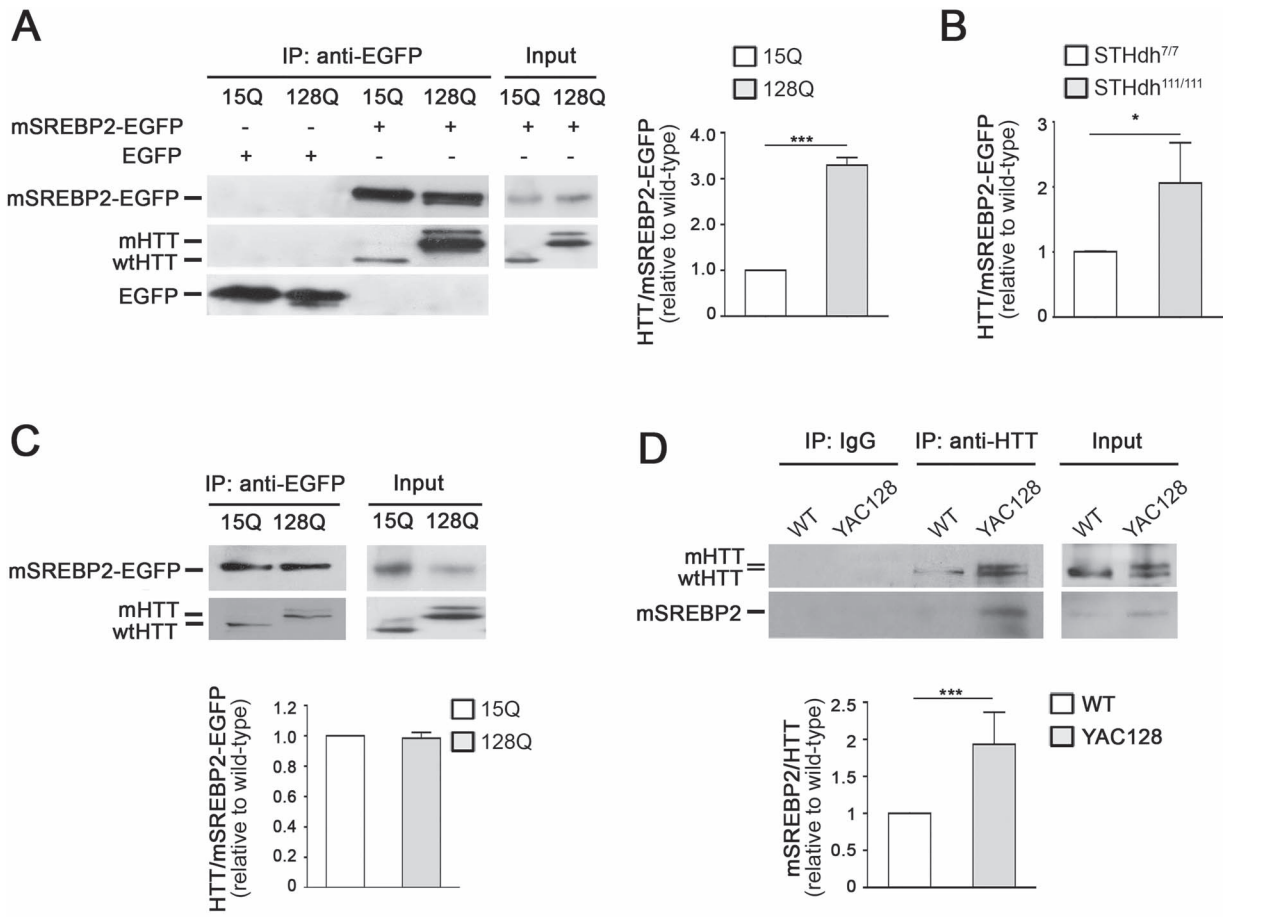

Figure 5. mSREBP2 co-immunoprecipitates with mHTT from cytoplasmic fractions of HD cells and brains. **(A)** mSREBP2-EGFP was transiently transfected into N548-15Q and N548-12Q cells and immunoprecipitated from cytoplasmic fractions using anti-EGFP antibodies. Mutant HTT was co-immunoprecipitated to a greater extent than wild-type HTT. No co-immunoprecipitation was detected in control samples expressing EGFP only. A representative immunoprecipitation is displayed, while the graph shows the densitometric analysis of 4 independent experiments. The amount of HTT co-immunoprecipitated was normalized over the amount mSREBP2-EGFP. **(B)** Densitometric analysis of HTT/mSREBP-EGFP co-immunoprecipitation from cytoplasmic fractions of STHdh$^{7/7}$ and STHdh$^{111/111}$ in three independent experiments (a representative immunoblot is shown in Figure 6B). **(C)** Both wild-type and mutant Htt co-immunoprecipitate with mSREBP2-EGFP from nuclear fractions of HD cells. mSREBP2-EGFP was immunoprecipitated from nuclear fractions using anti-GFP antibodies. The graph shows the densitometric analysis of 3 independent experiments. **(D)** Representative immunoblot and densitometric analysis of 3 independent experiments, each using different animals, showing co-immunoprecipitation of endogenous mSREBP2 with HTT from the cytoplasmic fraction of YAC128 cortical tissue. The amount of endogenous mSREBP2 co-immunoprecipitated was normalized over the amount of HTT. Data are mean values ± SD. Two-tailed *t*-test. $^{*}P < 0.05$; $^{***}P < 0.001$.

this was due to impaired SREBPs processing and generation of their transcriptionally active mature forms or to other potential mechanisms.

SREBPs are expressed as inactive precursors located in the ER membrane and are subjected to several levels of regulation (48). SCAP and COPII-mediated transport of SREBPs to the Golgi is crucial for proteolytic cleavage and release of the transcriptionally active mSREBPs (49). In our study, cortical and striatal levels of mSREBP2 were similar between 6-month-old wild-type and YAC128 mice, suggesting that SREBP transport to the Golgi and cleavage were not affected. However, we found that less mSREBP2 was present in nuclear fractions from HD brain cortex compared to wild-type due to abnormal re-distribution of the protein to cytoplasmic fractions. These data suggest that nuclear translocation and/or retention of mSREBP2, rather than processing, are affected in YAC128 mice. In HD striatal tissue, however, mSREBP2 subcellular distribution was similar to wild-type. This is in contrast to other studies that have shown changes in cholesterol synthesis in both cortex and striatum (10,30), and might be explained by mouse model- and strain-specific differences, or by an higher sensitivity of assays performed in other studies that measured the downstream consequences of mSREBP mislocalization, including gene transcripts or cholesterol metabolites. In wild-type mice, the rate of cholesterol synthesis was shown to be significantly higher in the cortex compared to the striatum (10). This could imply an overall higher activity of SREBP in the cortex and facilitate detection of changes in the subcellular distribution of mSREBP2.

In line with the results obtained by subcellular fractionation of cortical tissue, transient expression of an EGFP-tagged version of mSREBP2 in cell models showed mislocalization of the chimeric protein to the cytoplasm in several HD models, including striatal cell lines expressing mHTT, primary neurons from YAC128 mice and fibroblasts from HD patients, while in control wild-type cells mSREBP2-EGFP was mostly located in the nucleus.

Our data suggest that mSREBP2 is sequestered in the cytoplasm of HD cells through binding to soluble mHTT. Although we have not mapped the precise region/s of interaction, the N-terminal portion of mHTT must be involved, because expression of a mHTT fragment encompassing the first N-terminal 548 amino acid residues of the protein was sufficient to

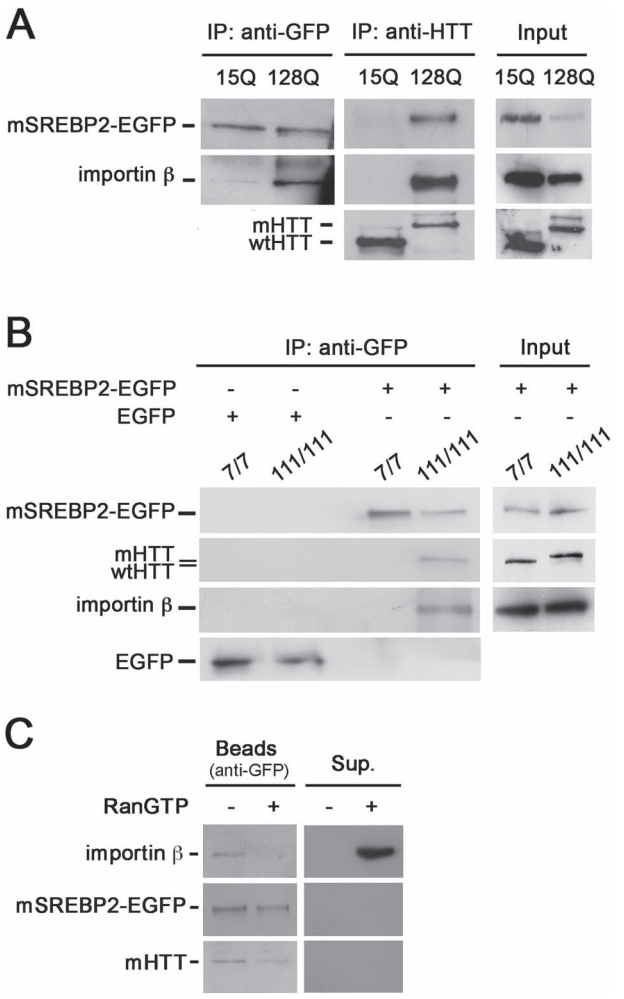

Figure 6. Mutant HTT is in a complex with mSREBP2 and importin ß and prevents their nuclear import. (**A**) Representative immunoblot showing that more importin ß co-immunoprecipitated with mSREBP2-EGFP from cytoplasmic fractions of N548-128Q cells than from cells N548-15Q cells, using anti-GFP antibodies. Importin ß is also co-immunoprecipitated by anti-HTT antibodies in a complex with mSREBP2-EGFP. The experiment was repeated three times with similar results. (**B**) Importin ß co-immunoprecipitated with mSREBP2-EGFP and full-length mHTT from STHdh$^{111/111}$ (111/111) cytoplasmic fractions, but not from STHdh$^{7/7}$ (7/7) fractions. (**C**) Representative immunoblot showing that RanGTP (5 μM) added to the mSREBP2-EGFP/mHTT/importin ß complex (immunoprecipitated with anti-GFP antibodies) triggered the release of importin ß from its cargo and into the supernatant. Mutant HTT remained in the pellet (beads), indicating that it does not directly interact with importin ß under these experimental conditions. The experiment was repeated twice with similar results.

co-immunoprecipitate mSREBP2 and disrupt its normal intracellular localization. The mHTT region that interacts with mSREBPs is likely to be located within the protein domain encoded by *HTT* exon 1, since decreased nuclear levels of mSREBPs and downregulation of the mevalonate pathway were reported in R6/2 mice (9), which express a short fragment of mHTT encoded by *HTT* exon 1 (50).

The mature forms of SREBPs translocate to the nucleus after dimerization and binding to one of the HEAT domains of importin β (37). Contrary to our expectations, mHTT did not impair binding of mSREBP2 to importin β. Rather, mHTT associated with and increased the cytoplasmic levels of mSREBP2/importin β complexes. These results, together with the observed increase in cytoplasmic levels of mSREBP2 in HD cells, lead us to conclude that mHTT impairs nuclear import of mSREBP2 and its release from importin β. We envisage three potential mechanisms that could give rise to this phenotype. In one scenario, mHTT could suppress the functions of the nuclear import machinery, including movement through the nuclear pore complex (NPC) or the RanGTP gradient across the nuclear envelope required for protein transport. This is a plausible explanation as previous reports have shown that NPCs are altered in cell and animal models of HD in an age- and gene-dosage dependent manner (51,52). Furthermore, the Ran GTPase-activating protein 1 (RanGAP1), which is crucial to the maintenance of the RanGTP gradient across the nuclear envelope, has been reported to be sequestered by mHTT aggregates, resulting in impaired nuclear transport (51,52). However, this explanation for the impaired import of mSREBP2 seems unlikely, as import of a NLS-GFP chimera, which would have been affected by defects in the nuclear transport machinery, occurred as effectively in HD cells as it did in wild-type cells (Fig. 3C). An alternative explanation for the inhibition of mSREBP2 nuclear localization was that binding of mHTT to the mSREBP2/importin β complex could, directly or indirectly, impair RanGTP-induced dissociation of importin β from mSREBP2, and thus prevent its accumulation in the nucleoplasm. However, this is also unlikely, as our *in vitro* experiments show that RanGTP can induce the release of importin β from the mHTT/mSREBP2-containing complex (Fig. 6C). This suggests that the impaired nuclear import of mSREBPs that we observed in HD cells is directly due to mHTT binding to the transcription factor in the cytoplasm, rather than to a general impairment of nucleocytoplasmic transport, and predates the onset of more general traffic problems. In HD cells mHTT/mSREBP2/importin β complexes remain localized in the cytoplasm, but not in mHTT insoluble aggregates (Fig. 4). This phenomenon must be saturable, since overexpression of mSREBP2-EGFP resulted in a significant amount of the chimeric protein entering the nucleus. However, mHTT binding to the limited amounts of mSREBPs produced by the cells in physiological conditions might prevent nuclear transport of a sufficient amount of transcription factor, and thus contribute to explain the decreased expression of SREBPs target genes in HD. In support of this hypothesis, in our studies, we observed a larger difference in HMGCR expression between wild-type and HD cells, when lower levels of transgenic mSREBP2 were expressed (Fig. 7A). Furthermore, HD cells showed impaired transcriptional response in conditions that are known to stimulate endogenous SREBP activity, including growth in sterol-deficient medium (LPDM) or in the presence of statins that inhibit HMGCR activity.

Different from what we observed in cytoplasmic fractions, both wild-type and mHTT were found to co-immunoprecipitate with mSREBP2 in similar amounts from nuclear fractions (Fig. 5C). This suggests that, in the nucleus, wild-type HTT (as well as mHTT) might be part of a transcriptional complex involved in the transcription of cholesterogenic genes in normal conditions. This would not be entirely surprising since wild-type HTT is known to associate with a number of transcription factors and regulators (53), including Sp1 (54), which is a transcriptional partner for SREBPs (55). In support of a potential role of wild-type HTT in the transcription of cholesterogenic genes, the activity of the mevalonate pathway was found to be increased in mice overexpressing wild-type HTT (YAC18) compared to mice expressing endogenous levels of HTT (8).

In our studies, both mSREBP2 and mSREBP1c were mislocalized to the cytoplasm in HD cells. Since these transcription

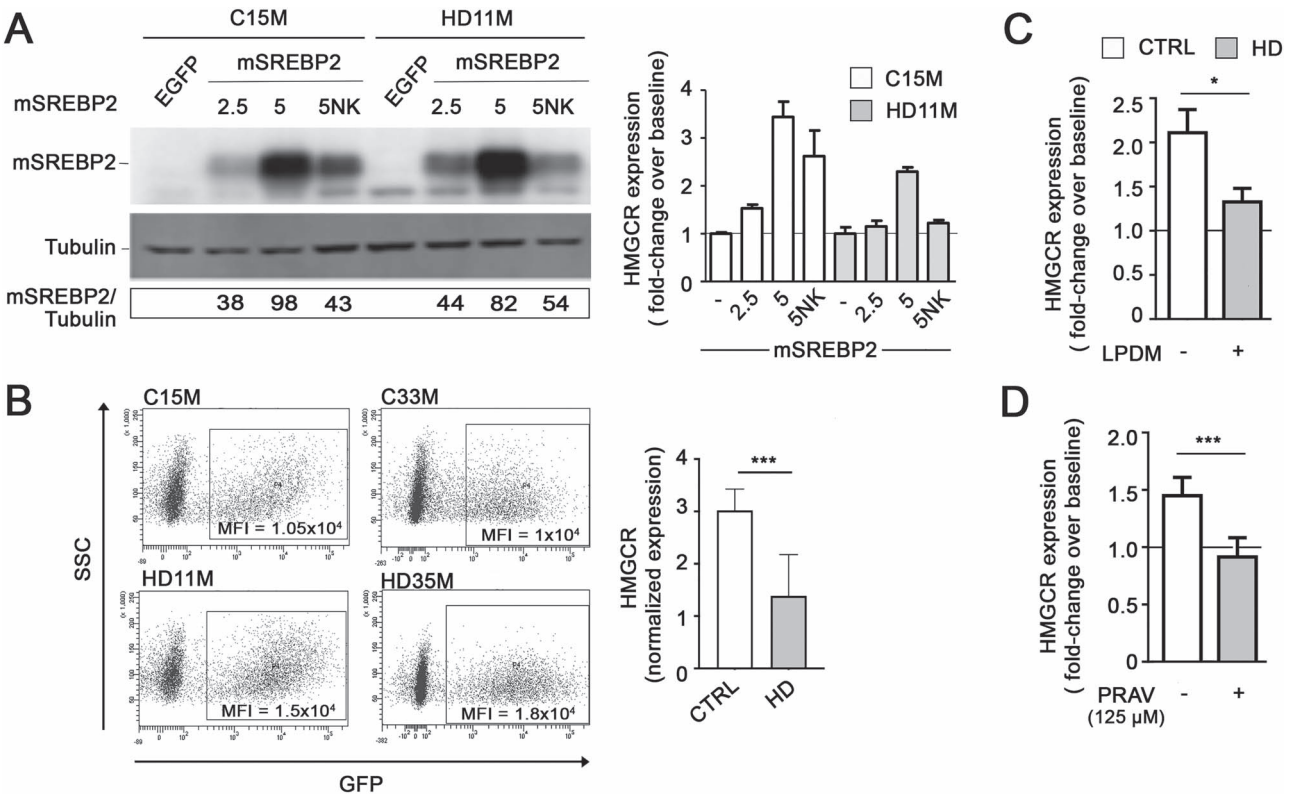

Figure 7. Impaired response of HD fibroblasts to mSREBP2 overexpression and to cholesterol deprivation. (**A**) *HMGCR* expression was measured in human primary fibroblasts transiently transfected with EGFP (baseline control) or with the indicated amounts of mSREBP2 cDNA (in μg). Cells were also transfected with the cDNA for mSREBP2 lacking the Kozak sequence (5 μg, 5NK), to allow for low transgene expression without compromising transfection efficiency. Transgene expression is shown in the immunoblot and in the relative densitometric data reported below, normalized over tubulin. C15M cells were from a healthy 15-year-old male subject, and HD11M cells were from a 11-year-old HD male patient. The graph shows fold-change expression of *HMGCR* over baseline. After each transfection, *HMGCR* expression was increased in HD cells to a lower extent than in control cells. Bars are means ± SD of three technical replicates per group. The horizontal line demarks baseline expression. (**B**) mSREBP2 was co-transfected with EGFP (10:1 ratio) in two control (C15M and C33M) and two HD (HD11M and HD35M) lines of human primary fibroblasts. Representative FACS scatter plots for transfected cells are shown. $EGFP^{+}$-cells (in the boxed area on the right end of each scatter plot) were sorted and used to measure *HMGCR* expression (shown in the graph). For each genotype, data from the two fibroblast lines, each analyzed in triplicate, were pooled together. MFI = Mean Fluorescence Intensity of EGFP-co-transfected cells. (**C**) *HMGCR* gene expression in human control and HD fibroblasts cultured in lipoprotein-deficient medium (LPDM) for 48 h. Values are expressed as fold-change compared to baseline expression in regular medium. Bars show mean values ± SD from three different fibroblast lines per genotype, each measured in triplicate. (**D**) *HMGCR* expression in control and HD fibroblasts treated with 125 μM pravastatin (PRAV) for 48 h. Bars show mean values ± SD from two different fibroblast lines per genotype, each measured in triplicate. Two-tailed *t*-test. $^{*}P < 0.05$; $^{***}P < 0.001$.

factors have been involved in several processes and metabolic pathways, our findings might have implications that extend beyond the mevalonate pathway and cholesterol synthesis, and might contribute to explain additional dysfunctions linked to HD. As an example, SREBP2 regulates the expression of a number of genes related to autophagy (56), a process of great importance for the clearance of toxic mHTT species in HD cells and involved in HD pathogenesis (57). On the other hand, the repertoire of mSREBP1 target genes spans from regulation of fatty acids and triacylglycerol metabolism to components of the insulin signaling pathway and iron homeostasis and ethanolamine kinase (required for the synthesis of phosphatidylethanolamine), among others (58,59). Of note, phosphoethanolamine—the product of ethanolamine kinase activity—was found to be decreased in the corpus striatum of HdhQ111/+ HD mice (60) and in the caudate of HD patients (61). Regulation of fatty acid synthesis by Drosophila SREBP was shown to be critical for neuronal dendritic arborization (62), a process that is affected in HD (63,64). SREBP1 can be activated by neuronal activity and is required for transcription of ARC (activity-regulated cytoskeleton-associated protein) (65), an immediate early gene involved in synaptic plasticity, the expression of which is decreased in an HD mouse model (66). Furthermore, SREBP1 maturation was shown to occur under conditions of NMDA receptor activation, and contributed to excitotoxicity in a stroke model (67). Although excitotoxicity is involved in HD pathogenesis, paradoxically old HD mice were shown to be resistant to excitotoxic stimuli (68). Whether this observation and the others mentioned above can be explained by the impairment of nuclear translocation of SREBP1 as described here remains to be determined.

In summary, our studies provide mechanistic insight on the dysfunction of the mevalonate pathway and cholesterol *de novo* synthesis in HD, and raise the question of whether additional pathways might be affected by the abnormal interaction of mHTT with mSREBPs.

Materials and Methods

Animal and cell models

YAC128 mice were maintained in our animal facility at the University of Alberta on FVB genetic background. All procedures on animals were approved by the University of Alberta's Animal

Care and Use Committee and were in accordance with the guidelines of the Canadian Council on Animal Care.

Conditionally-immortalized rat striatal ST14A cells and ST14A cells overexpressing an N-terminal fragment of mHTT (548 amino acids) containing 15 or 128 glutamines (N548-15Q and N548-128Q, respectively) were kindly provided by Dr. E. Cattaneo (University of Milan, Italy) and maintained in culture at the permissive temperature (33°C) as previously reported (69). Conditionally immortalized mouse striatal knock-in cells expressing endogenous full-length wild-type (ST*Hdh*$^{7/7}$) or mHTT (ST*Hdh*$^{111/111}$) were a gift from Dr. M.E. MacDonald (Massachusetts General Hospital, Boston, MA) and were maintained as previously described (70).

Human skin fibroblasts isolated from HD patients (lines GM03621, GM04208, GM04855 and GM05539 expressing one *HD* allele with 61, 45, 50 and 86 CAG repeats, respectively) or healthy controls (lines GM01869, AG08181 and AG07573) were purchased from the Coriell Cell Repositories (Coriell Institute for Medical Research, Camden, NJ) and grown in modified Eagle's Medium (MEM, Life Technologies, Carlsbad, CA) supplemented with 15% fetal bovine serum (FBS), 2 mM L-glutamine, 100 U/ml penicillin, 100 µg/ml streptomycin and 1 mM sodium pyruvate, unless otherwise indicated. Primary cortical neurons were prepared from newborn mice (P0). Briefly, brain tissue was minced and digested with 1 mg/ml papain for 15 min at 37°C. DNase was added to the digestion mix in the last 5 min of incubation. Cells were centrifuged at 200*g* for 1 min, resuspended in Neurobasal-A medium supplemented with 1% B27 (Life Technologies) and gently dissociated by pipetting up and down. Neurons were grown onto poly-L-lysine-coated coverslips at a density of 1×10^5 cells/cm^2.

Generation of mSREBP constructs

The cDNAs for the mature forms of human SREBP2 (amino acids 1–484) and human SREBP1c (amino acids 1–466) were obtained from HeLa cells by RT-PCR using the following primers: SREBP2-Fw (5′-AAACTCGAGCAATGGACGACAGCGGC-3′) and SREBP2-Rev (5′-GGGATCCTCACAGAAGAATCCGTGAGCG-3′); SREBP1c-Fw (5′-GCCTCGAGCAATGGATTGCACTTTC-3′) and SREBP1c-Rev (5′-TATGGATCCTCACAGGGCCAGGCGGGAG-3′). Forward primers included an XhoI restriction site upstream of the start codon, while reverse primers included a stop codon downstream to amino acid 484 in the human SREBP2 protein sequence, or amino acid 466 for SREBP1c (S2P cleavage sites), and BamH1 restriction site for in-frame directional cloning into pEGFP-C1 vector (Clontech, Mountain View, CA). The resulting plasmids (herein referred to as mSREBP2-EGFP and mSREBP1c-EGFP) encoding chimeric mSREBP proteins fused at the C-terminus of EGFP were sequenced to confirm cDNA sequence and cloning in frame with EGFP. The same PCR product, which lacks a classic Kozak sequence upstream of the start codon, was inserted into pcDNA3.1 hygro (–), to generate pcDNA-NK-mSREBP2 for attenuated expression of untagged mSREBP2. Finally, a canonical Kozak sequence was inserted into this construct by site-directed mutagenesis, to generate pcDNA-mSREBP2 for enhanced cDNA expression. NLS-EGFP plasmid was kindly donated by Dr. Luc Berthiaume (University of Alberta, Canada).

Cell transfection

Rat and mouse striatal cell lines were transiently transfected using Lipofectamine 2000 (Life Technologies) or SG Cell Line Nucleofector Kit (Lonza, Basel, Switzerland) according to the manufacturer's instructions. Primary fibroblasts were transfected using P2 Primary Nucleofector Kit. Cells were analyzed 12–24 h after transfection. Primary cortical and striatal neurons were transfected prior to plating, using the Mouse Neurons Nucleofector Kit (Lonza) according to the manufacturer's instructions. Briefly, 2×10^6 cells were suspended in 100 µl of Nucleofector reagent and 1 µg of plasmid was added for nucleofection. Electroporated neurons were immediately plated on coverslips previously coated with poly-L-lysine and cultured for 36 h at 37°C before confocal microscopy analysis.

Subcellular fractionation

Two hours prior to cell collection and lysis, 25 µg/ml N-acetyl-leucyl-leucyl-norleucinal (ALLN) was added to the cell culture medium. Cells and freshly isolated brain tissue were homogenized in buffer A (10 mM HEPES-K^+ pH 7.5, 250 mM sucrose, 10 mM KCl, 1.5 mM $MgCl_2$, 1 mM EDTA, 1 mM EGTA and Protease-Inhibitor Cocktail, all from Sigma), by passing the cells 20 times through a 26-G syringe needle. Cell lysates were incubated on ice for 20 min and then centrifuged at 1000*g* for 5 min. The supernatant (cytoplasmic fraction) was harvested and stored at −80°C until use. The nuclear pellet was washed once with buffer A and then resuspended in buffer B (20 mM HEPES-K^+ pH 7.9, 420 mM NaCl, 0.2 mM EDTA, 1.5 mM $MgCl_2$, 25% glycerol) and incubated for 1 h at 4°C on a shaker. Following centrifugation at 20 000*g* for 1 h at 4°C, the supernatant (nuclear extract) was collected and stored at −80°C until use. About 20–30 µg of total, cytoplasmic and nuclear proteins were resolved on 10% SDS-PAGE and immunoblotted as indicated below.

Immunoprecipitation

Immunoprecipitation of transfected mSREBP2-EGFP was performed from cytoplasmic (0.8 mg) and nuclear (0.4 mg) fractions, using goat anti-EGFP antibodies (a gift from Dr. Luc Berthiaume, University of Alberta, Canada). HTT was immunoprecipitated from cytoplasmic fractions from WT and YAC128 mouse brain using a cocktail of anti-HTT antibodies mAb2166 and mAb2168 (Millipore, Burlington, MA). Antibodies were complexed to protein G-Sepharose beads (Invitrogen) overnight at 4°C, before incubation with cytoplasmic or nuclear fractions for 4 h at RT. Immunoprecipitated complexes were resolved on SDS-PAGE and detected by immunoblotting with anti-HTT (mAb2166 1:5000, Millipore), anti-EGFP (1:1000), anti-SREBP2 (1:1000, Abcam) and anti-importin β (1:1000, Sigma) antibodies.

Immunoblotting

Proteins were resolved on 10% SDS-PAGE and transferred to nitrocellulose membranes (Bio-Rad Laboratories, Hercules, CA). Membranes were blocked with 5% non-fat milk in TBS-T buffer or with 5% BSA in TBS-T buffer for 1 h at room temperature and then incubated overnight at 4°C with the following primary antibodies: anti-SREBP2 (rabbit polyclonal, 1:1000, Abcam), anti-β-tubulin (mouse monoclonal, 1:1000, Cell Signaling), anti-histone 1 (rabbit polyclonal, 1:1000, Santa Cruz) or anti-lamin A/C (rabbit polyclonal, 1:1000, Cell Signaling). Incubation with HRP- or IRDye-conjugated secondary antibodies was performed for 1 h at RT. Detection of HRP signal was performed using ECL Plus (GE Healthcare, Boston, MA), while infrared fluorescence was measured with an Odyssey infrared imaging system (LI-COR).

Detection of mutant HTT aggregates and filter-trap assay

Cell lysates from WT and HD cells transfected with EGFP-mSREBP2 were prepared as described above. Thirty µg of total or cytoplasmic cellular proteins were resolved on 6% SDS-PAGE and both stacking and resolving gel were transferred to nitrocellulose membrane (Bio-Rad Laboratories) for immunoblotting. SDS-insoluble mutant HTT aggregates were detected in the stacking gel by immunoblotting with anti-HTT antibodies (mAb2166, Millipore). Goat anti-GFP was used to probe for mSREBP2-EGFP. For the filter trap assay, cytoplasmic cell fractions were centrifuged at 13 000*g* for 10 min. The resulting pellet was resuspended in 2% SDS, incubated for 15 min at RT and sonicated for 10 s, before being filtered through a cellulose acetate membrane (0.2-µm pore size, Schleicher and Schuell), using a dot-blot filtration unit (Bio-Rad Laboratories). SDS-insoluble aggregates retained on the membrane after washing with 1% SDS in PBS were detected with anti-HTT antibodies (mAB2166, 1:1000, Millipore) and goat anti-GFP, followed by incubation with secondary HRP-conjugated antibodies (1:10 000, BioRad) and ECL chemiluminescence detection (GE Healthcare).

Immunocytochemistry and confocal microscopy

About 24–36 h after transfection with the indicated plasmids, cells were washed with PBS, fixed in 4% paraformaldehyde for 10 min at RT and permeabilized with 0.5% Triton X-100 in PBS for 5 min. After blocking with 4% donkey serum for 1 h at RT, cells were incubated with anti-HTT antibodies (mAb2166 and EM48, 1:500, Millipore; PW0595, 1:500, Enzo), followed by Alexa 555-conjugated secondary antibodies (1:500, Life Technologies). Nuclei were counterstained with 4′,6-diamidino-2-phenylindole (DAPI, Vector Laboratories, Burlingame, CA) for 10 min at RT. Coverslips were mounted using ProLong Gold antifade reagent (Life Technologies) and analyzed with an LSM510 laser scanning confocal microscope mounted on a Zeiss Axiovert 100 M microscope, using a 100X or 63X oil immersion lens. Images were acquired using the same confocal settings across all samples. A minimum of 100 cells were analyzed to determine the percentage of cells with cytoplasmic localization of mSREBP2-EGFP. Analysis of colocalization was performed using ZEN 2009 software.

High content analysis of NLS-EGFP localization

N548-15Q and N548-128Q cells were transfected by electroporation with NLS-EGFP plasmid, using SG Cell Line 4D-Nucleofector ™ kit (Lonza), and then seeded into glass-bottom 96-well plates, in triplicate. Fifteen fields per well were acquired using Operetta High-Content Imaging System (PerkinElmer, Waltham, MA) with 20X magnification. The number of cells with NLS-EGFP localized to the cytoplasm was quantified using Harmony 4.1 software (PerkinElmer).

RanGTP preparation and binding assay

RanGTP was prepared as previously described (71). Purified RanGTP (5 µM in PBS) was incubated for 1 h at RT with the mSREBP2-EGFP/mHTT/importin β complex immunoprecipitated with anti-EGFP antibodies and protein G-Sepharose. Importin β released in the supernatant was detected by immunoblotting.

Preparation of lipoprotein-deficient serum

Potassium bromide was added to 50 ml of FBS until a density of 1.215 g/ml was reached. FBS was centrifuged at 286 000*g* for 24 h at 8°C in an Opti-MAX Tabletop Ultracentrifuge (Beckman Coulter, Brea, CA) using an MLA-55 rotor. Floating lipoproteins were removed with a pipette and the remaining lipoprotein-deficient serum was dialyzed against 100 volumes of dialysis buffer (150 mM NaCl, 1 mM EDTA, 5 mM Tris-HCl pH 7.4), using a 12–14 KDa molecular weight cut-off dialysis membrane. Dialysis buffer was replaced three times over the course of 48 h. After dialysis, the lipoprotein-deficient serum was filter-sterilized using a 0.2 µm pore size nitrocellulose membrane. The extent of delipidation (>92% for the serum used in this study) was determined by measuring cholesterol concentration before and after lipoprotein flotation, using the Amplex Red Cholesterol Assay Kit (Life Technologies). Control serum underwent the same procedure as above, except for the centrifugation step.

Quantitative PCR

Total RNA was extracted using RNeasy® or RNeasy® Micro kits (Qiagen, Venlo, Netherlands) according to the manufacturer's instructions. All RNA samples were subjected to in-column treatment with DNase I (Qiagen) to eliminate genomic DNA contamination. 0.5–2 µg of total RNA were reverse-transcribed using Superscript II reverse transcriptase (Life Technologies) and oligo-d(T) primer, and the resulting cDNAs were amplified using Power SYBR® Green PCR Master Mix (Applied Biosystems, Foster City, CA, USA), following manufacturer' instructions. Quantitative PCR analysis was carried out on a StepOnePlus™ instrument (Applied Biosystems, Foster City, CA), by comparison with a standard curve generated by cDNA serial dilutions. Gene-specific primers were designed using Primer Express 3.0 software (Applied Biosystems) or the Assay Design Center online software (Roche, Basel, Switzerland). Unless otherwise indicated, gene expression was normalized over the geometric mean of the expression levels of the three most stable housekeeping genes: *ATP5B, EIF4A2 and 36B4* (72).

Acknowledgements

This work was supported by grants from the Canadian Institutes for Health Research (CIHR MOP 111219) and from the Huntington Society of Canada to SS. ADP and LCM were supported by Alberta Innovates Health Solution (AIHS) Studentships. LCM was supported by a COLCIENCIAS (Colombia) Studentship. JM was supported by a CIHR Banting and Best Canada Graduate Scholarship-Master's. SS was supported by a Tier 2 Canada Research Chair and AIHS Scholarship. Experiments were performed at the University of Alberta Faculty of Medicine and Dentistry Cell Imaging Centre, Flow Cytometry Core and High Content Analysis Core, which receive financial support from the Faculty of Medicine and Dentistry and Canada Foundation for Innovation (CFI) awards to contributing investigators. The Cell Imaging Centre and the High content Analysis Core receive additional financial support from the Department of Medical Microbiology and Immunology and the Li Ka Shing Institute of Virology, respectively.

Conflict of interest statement: The authors declare no conflict of interest.

References

1. (1993) A novel gene containing a trinucleotide repeat that is expanded and unstable on Huntington's disease chromosomes. The Huntington's disease collaborative research group. *Cell*, **72**, 971–983.
2. Roos, R.A. (2010) Huntington's disease: a clinical review. *Orphanet J. Rare Dis.*, **5**, 40.
3. Ha, A.D. and Fung, V.S. (2012) Huntington's disease. *Curr. Opin. Neurol.*, **25**, 491–498.
4. Zheng, Z. and Diamond, M.I. (2012) Huntington disease and the huntingtin protein. *Prog. Mol. Biol. Transl. Sci.*, **107**, 189–214.
5. Imarisio, S., Carmichael, J., Korolchuk, V., Chen, C.W., Saiki, S., Rose, C., Krishna, G., Davies, J.E., Ttofi, E., Underwood, B.R. *et al.* (2008) Huntington's disease: from pathology and genetics to potential therapies. *Biochem. J.*, **412**, 191–209.
6. Sipione, S., Rigamonti, D., Valenza, M., Zuccato, C., Conti, L., Pritchard, J., Kooperberg, C., Olson, J.M. and Cattaneo, E. (2014) Early transcriptional profiles in huntingtin-inducible striatal cells by microarray analyses. *Hum. Mol. Genet.*, in press.
7. Valenza, M., Leoni, V., Tarditi, A., Mariotti, C., Bjorkhem, I., Di Donato, S. and Cattaneo, E. (2007) Progressive dysfunction of the cholesterol biosynthesis pathway in the R6/2 mouse model of Huntington's disease. *Neurobiol. Dis.*, **28**, 133–142.
8. Valenza, M., Carroll, J.B., Leoni, V., Bertram, L.N., Bjorkhem, I., Singaraja, R.R., Di Donato, S., Lutjohann, D., Hayden, M.R. and Cattaneo, E. (2007) Cholesterol biosynthesis pathway is disturbed in YAC128 mice and is modulated by huntingtin mutation. *Hum. Mol. Genet.*, **16**, 2187–2198.
9. Valenza, M., Rigamonti, D., Goffredo, D., Zuccato, C., Fenu, S., Jamot, L., Strand, A., Tarditi, A., Woodman, B., Racchi, M. *et al.* (2005) Dysfunction of the cholesterol biosynthetic pathway in Huntington's disease. *J. Neurosci.*, **25**, 9932–9939.
10. Shankaran, M., Di Paolo, E., Leoni, V., Caccia, C., Ferrari Bardile, C., Mohammed, H., Di Donato, S., Kwak, S., Marchionini, D., Turner, S. *et al.* (2017) Early and brain region-specific decrease of de novo cholesterol biosynthesis in Huntington's disease: a cross-validation study in Q175 knock-in mice. *Neurobiol. Dis.*, **98**, 66–76.
11. Faust, J.R., Goldstein, J.L. and Brown, M.S. (1979) Synthesis of ubiquinone and cholesterol in human fibroblasts: regulation of a branched pathway. *Arch. Biochem. Biophys.*, **192**, 86–99.
12. Butterworth, P.H., Draper, H.H., Hemming, F.W. and Morton, R.A. (1966) In vivo incorporation of [2-14-C]-mevalonate into dolichol of rabbit and pig liver. *Arch. Biochem. Biophys.*, **113**, 646–653.
13. Hooff, G.P., Wood, W.G., Muller, W.E. and Eckert, G.P. (2010) Isoprenoids, small GTPases and Alzheimer's disease. *Biochim. Biophys. Acta*, **1801**, 896–905.
14. Dietschy, J.M. and Turley, S.D. (2004) Thematic review series: brain lipids. Cholesterol metabolism in the central nervous system during early development and in the mature animal. *J. Lipid Res.*, **45**, 1375–1397.
15. Charalampopoulos, I., Remboutsika, E., Margioris, A.N. and Gravanis, A. (2008) Neurosteroids as modulators of neurogenesis and neuronal survival. *Trends Endocrinol. Metab.*, **19**, 300–307.
16. Puia, G., Santi, M.R., Vicini, S., Pritchett, D.B., Purdy, R.H., Paul, S.M., Seeburg, P.H. and Costa, E. (1990) Neurosteroids act on recombinant human GABAA receptors. *Neuron*, **4**, 759–765.
17. Borochov, H., Abbott, R.E., Schachter, D. and Shinitzky, M. (1979) Modulation of erythrocyte membrane proteins by membrane cholesterol and lipid fluidity. *Biochemistry*, **18**, 251–255.
18. George, K.S. and Wu, S. (2012) Lipid raft: a floating island of death or survival. *Toxicol. Appl. Pharmacol.*, **259**, 311–319.
19. Sonnino, S. and Prinetti, A. (2016) The role of sphingolipids in neuronal plasticity of the brain. *J. Neurochem.*, **137**, 485–488.
20. Sonnino, S., Aureli, M., Mauri, L., Ciampa, M.G. and Prinetti, A. (2015) Membrane lipid domains in the nervous system. *Front. Biosci., Landmark Ed.*, **20**, 280–302.
21. Pfrieger, F.W. (2003) Cholesterol homeostasis and function in neurons of the central nervous system. *Cell. Mol. Life Sci.*, **60**, 1158–1171.
22. Thiele, C., Hannah, M.J., Fahrenholz, F. and Huttner, W.B. (2000) Cholesterol binds to synaptophysin and is required for biogenesis of synaptic vesicles. *Nat. Cell Biol.*, **2**, 42–49.
23. Mitter, D., Reisinger, C., Hinz, B., Hollmann, S., Yelamanchili, S.V., Treiber-Held, S., Ohm, T.G., Herrmann, A. and Ahnert-Hilger, G. (2003) The synaptophysin/synaptobrevin interaction critically depends on the cholesterol content. *J. Neurochem.*, **84**, 35–42.
24. Lang, T., Bruns, D., Wenzel, D., Riedel, D., Holroyd, P., Thiele, C. and Jahn, R. (2001) SNAREs are concentrated in cholesterol-dependent clusters that define docking and fusion sites for exocytosis. *EMBO J.*, **20**, 2202–2213.
25. Mauch, D.H., Nagler, K., Schumacher, S., Goritz, C., Muller, E.C., Otto, A. and Pfrieger, F.W. (2001) CNS synaptogenesis promoted by glia-derived cholesterol. *Science*, **294**, 1354–1357.
26. Courtney, R. and Landreth, G.E. (2016) LXR regulation of brain cholesterol: from development to disease. *Trends Endocrinol. Metab.*, **27**, 404–414.
27. Bjorkhem, I. and Meaney, S. (2004) Brain cholesterol: long secret life behind a barrier. *Arterioscler. Thromb. Vasc. Biol.*, **24**, 806–815.
28. Martin, M.G., Pfrieger, F. and Dotti, C.G. (2014) Cholesterol in brain disease: sometimes determinant and frequently implicated. *EMBO Rep.*, **15**, 1036–1052.
29. Vance, J.E. (2012) Dysregulation of cholesterol balance in the brain: contribution to neurodegenerative diseases. *Dis. Model. Mech.*, **5**, 746–755.
30. Kreilaus, F., Spiro, A.S., Hannan, A.J., Garner, B. and Jenner, A.M. (2015) Brain cholesterol synthesis and metabolism is progressively disturbed in the R6/1 mouse model of Huntington's disease: a targeted GC-MS/MS sterol analysis. *J. Huntington's Dis.*, **4**, 305–318.
31. Valenza, M., Marullo, M., Di Paolo, E., Cesana, E., Zuccato, C., Biella, G. and Cattaneo, E. (2015) Disruption of astrocyte-neuron cholesterol cross talk affects neuronal function in Huntington's disease. *Cell Death Differ.*, **22**, 690–702.
32. Valenza, M., Chen, J.Y., Di Paolo, E., Ruozi, B., Belletti, D., Ferrari Bardile, C., Leoni, V., Caccia, C., Brilli, E., Di Donato, S. *et al.* (2015) Cholesterol-loaded nanoparticles ameliorate synaptic and cognitive function in Huntington's disease mice. *EMBO Mol. Med.*, **7**, 1547–1564.
33. Horton, J.D., Goldstein, J.L. and Brown, M.S. (2002) SREBPs: activators of the complete program of cholesterol and fatty acid synthesis in the liver. *J. Clin. Invest.*, **109**, 1125–1131.
34. Horton, J.D., Shah, N.A., Warrington, J.A., Anderson, N.N., Park, S.W., Brown, M.S. and Goldstein, J.L. (2003) Combined analysis of oligonucleotide microarray data from transgenic and knockout mice identifies direct SREBP target genes. *Proc. Natl. Acad. Sci. U. S. A.*, **100**, 12027–12032.
35. Nohturfft, A., DeBose-Boyd, R.A., Scheek, S., Goldstein, J.L. and Brown, M.S. (1999) Sterols regulate cycling of SREBP

cleavage-activating protein (SCAP) between endoplasmic reticulum and Golgi. *Proc. Natl. Acad. Sci. U. S. A.*, **96**, 11235–11240.
36. Duncan, E.A., Dave, U.P., Sakai, J., Goldstein, J.L. and Brown, M.S. (1998) Second-site cleavage in sterol regulatory element-binding protein occurs at transmembrane junction as determined by cysteine panning. *J. Biol. Chem.*, **273**, 17801–17809.
37. Nagoshi, E., Imamoto, N., Sato, R. and Yoneda, Y. (1999) Nuclear import of sterol regulatory element-binding protein-2, a basic helix-loop-helix-leucine zipper (bHLH-zip)-containing transcription factor, occurs through the direct interaction of importin beta with HLH-zip. *Mol. Biol. Cell*, **10**, 2221–2233.
38. Nagoshi, E. and Yoneda, Y. (2001) Dimerization of sterol regulatory element-binding protein 2 via the helix-loop-helix-leucine zipper domain is a prerequisite for its nuclear localization mediated by importin beta. *Mol. Cell. Biol.*, **21**, 2779–2789.
39. Lee, S.J., Sekimoto, T., Yamashita, E., Nagoshi, E., Nakagawa, A., Imamoto, N., Yoshimura, M., Sakai, H., Chong, K.T., Tsukihara, T. *et al.* (2003) The structure of importin-beta bound to SREBP-2: nuclear import of a transcription factor. *Science*, **302**, 1571–1575.
40. Slow, E.J., van Raamsdonk, J., Rogers, D., Coleman, S.H., Graham, R.K., Deng, Y., Oh, R., Bissada, N., Hossain, S.M., Yang, Y.Z. *et al.* (2003) Selective striatal neuronal loss in a YAC128 mouse model of Huntington disease. *Hum. Mol. Genet.*, **12**, 1555–1567.
41. Sipione, S., Rigamonti, D., Valenza, M., Zuccato, C., Conti, L., Pritchard, J., Kooperberg, C., Olson, J.M. and Cattaneo, E. (2002) Early transcriptional profiles in huntingtin-inducible striatal cells by microarray analyses. *Hum. Mol. Genet.*, **11**, 1953–1965.
42. Zuccato, C., Valenza, M. and Cattaneo, E. (2010) Molecular mechanisms and potential therapeutical targets in Huntington's disease. *Physiol. Rev.*, **90**, 905–981.
43. Yoshimura, S.H. and Hirano, T. (2016) HEAT repeats - versatile arrays of amphiphilic helices working in crowded environments? *J. Cell Sci.*, **129**, 3963–3970.
44. Guo, Q., Bin, H., Cheng, J., Seefelder, M., Engler, T., Pfeifer, G., Oeckl, P., Otto, M., Moser, F., Maurer, M. *et al.* (2018) The cryo-electron microscopy structure of huntingtin. *Nature*, **555**, 117–120.
45. Kozak, M. (1987) An analysis of 5′-noncoding sequences from 699 vertebrate messenger RNAs. *Nucleic Acids Res.*, **15**, 8125–8148.
46. Hua, X., Yokoyama, C., Wu, J., Briggs, M.R., Brown, M.S., Goldstein, J.L. and Wang, X. (1993) SREBP-2, a second basic-helix-loop-helix-leucine zipper protein that stimulates transcription by binding to a sterol regulatory element. *Proc. Natl. Acad. Sci. U. S. A.*, **90**, 11603–11607.
47. Yokoyama, C., Wang, X., Briggs, M.R., Admon, A., Wu, J., Hua, X., Goldstein, J.L. and Brown, M.S. (1993) SREBP-1, a basic-helix-loop-helix-leucine zipper protein that controls transcription of the low density lipoprotein receptor gene. *Cell*, **75**, 187–197.
48. Jeon, T.I. and Osborne, T.F. (2012) SREBPs: metabolic integrators in physiology and metabolism. *Trends Endocrinol. Metab.*, **23**, 65–72.
49. Brown, M.S., Radhakrishnan, A. and Goldstein, J.L. (2018) Retrospective on cholesterol homeostasis: the central role of Scap. *Annu. Rev. Biochem.*, **87**, 783–807.
50. Mangiarini, L., Sathasivam, K., Seller, M., Cozens, B., Harper, A., Hetherington, C., Lawton, M., Trottier, Y., Lehrach, H., Davies, S.W. *et al.* (1996) Exon 1 of the HD gene with an expanded CAG repeat is sufficient to cause a progressive neurological phenotype in transgenic mice. *Cell*, **87**, 493–506.
51. Grima, J.C., Daigle, J.G., Arbez, N., Cunningham, K.C., Zhang, K., Ochaba, J., Geater, C., Morozko, E., Stocksdale, J., Glatzer, J.C. *et al.* (2017) Mutant Huntingtin disrupts the nuclear pore complex. *Neuron*, **94**, 93, e106–107.
52. Gasset-Rosa, F., Chillon-Marinas, C., Goginashvili, A., Atwal, R.S., Artates, J.W., Tabet, R., Wheeler, V.C., Bang, A.G., Cleveland, D.W. and Lagier-Tourenne, C. (2017) Polyglutamine-expanded Huntingtin exacerbates age-related disruption of nuclear integrity and Nucleocytoplasmic transport. *Neuron*, **94**, 48, e44–57.
53. Saudou, F. and Humbert, S. (2016) The biology of Huntingtin. *Neuron*, **89**, 910–926.
54. Dunah, A.W., Jeong, H., Griffin, A., Kim, Y.M., Standaert, D.G., Hersch, S.M., Mouradian, M.M., Young, A.B., Tanese, N. and Krainc, D. (2002) Sp1 and TAFII130 transcriptional activity disrupted in early Huntington's disease. *Science*, **296**, 2238–2243.
55. Sanchez, H.B., Yieh, L. and Osborne, T.F. (1995) Cooperation by sterol regulatory element-binding protein and Sp1 in sterol regulation of low density lipoprotein receptor gene. *J. Biol. Chem.*, **270**, 1161–1169.
56. Seo, Y.K., Jeon, T.I., Chong, H.K., Biesinger, J., Xie, X. and Osborne, T.F. (2011) Genome-wide localization of SREBP-2 in hepatic chromatin predicts a role in autophagy. *Cell Metab.*, **13**, 367–375.
57. Croce, K.R. and Yamamoto, A. (2019) A role for autophagy in Huntington's disease. *Neurobiol. Dis.*, **122**, 16–22.
58. Reed, B.D., Charos, A.E., Szekely, A.M., Weissman, S.M. and Snyder, M. (2008) Genome-wide occupancy of SREBP1 and its partners NFY and SP1 reveals novel functional roles and combinatorial regulation of distinct classes of genes. *PLoS Genet.*, **4**, e1000133.
59. Xiaoli, A.M., Song, Z. and Yang, F. (2019) Lipogenic SREBP-1a/c transcription factors activate expression of the iron regulator hepcidin, revealing cross-talk between lipid and iron metabolisms. *J. Biol. Chem.*, **294**, 12743–12753.
60. Carroll, J.B., Deik, A., Fossale, E., Weston, R.M., Guide, J.R., Arjomand, J., Kwak, S., Clish, C.B. and MacDonald, M.E. (2015) HdhQ111 mice exhibit tissue specific metabolite profiles that include striatal lipid accumulation. *PLoS One*, **10**, e0134465.
61. Ellison, D.W., Beal, M.F. and Martin, J.B. (1987) Phosphoethanolamine and ethanolamine are decreased in Alzheimer's disease and Huntington's disease. *Brain Res.*, **417**, 389–392.
62. Ziegler, A.B., Thiele, C., Tenedini, F., Richard, M., Leyendecker, P., Hoermann, A., Soba, P. and Tavosanis, G. (2017) Cell-autonomous control of neuronal dendrite expansion via the fatty acid synthesis regulator SREBP. *Cell Rep.*, **21**, 3346–3353.
63. Lerner, R.P., Trejo Martinez Ldel, C., Zhu, C., Chesselet, M.F. and Hickey, M.A. (2012) Striatal atrophy and dendritic alterations in a knock-in mouse model of Huntington's disease. *Brain Res. Bull.*, **87**, 571–578.
64. Kweon, J.H., Kim, S. and Lee, S.B. (2017) The cellular basis of dendrite pathology in neurodegenerative diseases. *BMB Rep.*, **50**, 5–11.
65. Chen, Y., Bang, S., McMullen, M.F., Kazi, H., Talbot, K., Ho, M.X., Carlson, G., Arnold, S.E., Ong, W.Y. and Kim, S.F. (2017) Neuronal activity-induced sterol regulatory element binding Protein-1 (SREBP1) is disrupted in Dysbindin-null

mice-potential link to cognitive impairment in schizophrenia. *Mol. Neurobiol.*, **54**, 1699–1709.
66. Giralt, A., Puigdellivol, M., Carreton, O., Paoletti, P., Valero, J., Parra-Damas, A., Saura, C.A., Alberch, J. and Gines, S. (2012) Long-term memory deficits in Huntington's disease are associated with reduced CBP histone acetylase activity. *Hum. Mol. Genet.*, **21**, 1203–1216.
67. Taghibiglou, C., Martin, H.G., Lai, T.W., Cho, T., Prasad, S., Kojic, L., Lu, J., Liu, Y., Lo, E., Zhang, S. *et al.* (2009) Role of NMDA receptor-dependent activation of SREBP1 in excitotoxic and ischemic neuronal injuries. *Nat. Med.*, **15**, 1399–1406.
68. Graham, R.K., Pouladi, M.A., Joshi, P., Lu, G., Deng, Y., Wu, N.P., Figueroa, B.E., Metzler, M., Andre, V.M., Slow, E.J. *et al.* (2009) Differential susceptibility to excitotoxic stress in YAC128 mouse models of Huntington disease between initiation and progression of disease. *J. Neurosci.*, **29**, 2193–2204.
69. Rigamonti, D., Bauer, J.H., De-Fraja, C., Conti, L., Sipione, S., Sciorati, C., Clementi, E., Hackam, A., Hayden, M.R., Li, Y. *et al.* (2000) Wild-type huntingtin protects from apoptosis upstream of caspase-3. *J. Neurosci.*, **20**, 3705–3713.
70. Trettel, F., Rigamonti, D., Hilditch-Maguire, P., Wheeler, V.C., Sharp, A.H., Persichetti, F., Cattaneo, E. and MacDonald, M.E. (2000) Dominant phenotypes produced by the HD mutation in STHdh(Q111) striatal cells. *Hum. Mol. Genet.*, **9**, 2799–2809.
71. Cairo, L.V. and Wozniak, R.W. (2016) The nuclear transport factor Kap121 is required for stability of the Dam1 complex and mitotic kinetochore bi-orientation. *Cell Rep.*, **14**, 2440–2450.
72. Vandesompele, J., De Preter, K., Pattyn, F., Poppe, B., Van Roy, N., De Paepe, A. and Speleman, F. (2002) Accurate normalization of real-time quantitative RT-PCR data by geometric averaging of multiple internal control genes. *Genome Biol.*, **3**, RESEARCH0034.